Interface-layer formation mechanism in a-Si:H thin-film growth studied by real-time spectroscopic ellipsometry and infrared spectroscopy

H. Fujiwara, Y. Toyoshima, M. Kondo, and A. Matsuda

Thin Film Silicon Solar Cells Super Laboratory, Electrotechnical Laboratory, 1-1-4 Umezono, Tsukuba-shi, Ibaraki 305-8568, Japan
(Received 14 July 1999)

Real-time spectroscopic ellipsometry (SE) and infrared attenuated total reflection spectroscopy (ATR) have been applied to investigate interface layer formation mechanisms in an a-Si:H film on a c-Si substrate covered with native oxide ($\sim$30 Å) in a conventional rf plasma-enhanced chemical vapor deposition. These real-time monitoring techniques allow us to determine a depth profile of hydrogen content for the SiH and SiH$_2$ bonding states, together with the microscopic structural evolution during the a-Si:H deposition. The analyses of these real-time measurements show the formation of a 35-Å-thick H-rich layer having an average hydrogen content of $\sim$17 at. % at the a-Si:H/substrate interface. A deuterium diffusion experiment performed after a 130-Å-thick a-Si:H deposition supports the H-rich layer formation at the interface. This interface layer formation is primarily caused by the H-rich three-dimensional island growth on the substrate in the early a-Si:H deposition stage. In a following coalescence process, we found a significant reduction in the hydrogen content in a-Si:H bulk layer, accompanied by a clear surface smoothening of the a-Si:H layer. The above results indicate that surface diffusion of precursors promotes a dense a-Si:H network formation during the coalescence and confines H-rich a-Si:H islands at the film/substrate interface region. [S0163-1829(99)01944-X]

I. INTRODUCTION

The importance of the interface control in a-Si:H based solar cells has long been recognized for the further optimization of solar cell performance.[1–3] Various attempts have been made to control p/i interface structures by the introduction of a thin buffer layer[1–2] or plasma treatment.[3] Although higher solar cell performances have been reported in these solar cells, a clear mechanism for such improvement has not been addressed in part owing to the lack of proper characterization techniques of very thin interface layers ($<$50 Å). The characterization of such an interface structure is, therefore, of significant importance for the further improvement of solar cell performance.

Recent developments in real time growth monitoring techniques including the spectroscopic ellipsometry (SE) and infrared spectroscopy enable us to characterize such thin interface structures on the atomic scale.[4–14] In the last decade, several articles have been devoted to the interface layer characterization in a-Si:H deposition using infrared (IR) spectroscopy.[4–9] In our earlier works using infrared reflection absorption spectroscopy (IRRAS), we obtained evidences of the H-rich interface layer formation on an Al substrate.[4,5] Later, similar H-rich layer formations in the early stage of a-Si:H deposition were reported on glass,[6] native oxide-covered c-Si,[7] and a-Si$_{1-x}$C$_x$:H substrates.[8,9] In these reports, however, the interface layer formation mechanisms in a-Si:H deposition are still controversial. The difficulties in interface layer characterization using IR spectroscopy mainly arise from the lack of detailed structural information on the depositing film. In addition, the problem of obtaining an accurate thickness from the IR spectra sometimes induces an ambiguity for the data interpretation.

Real time SE performed in the UV/visible range provides

a perfect tool to obtain such microscopic structural information during the interface formation.[10–13] This technique has been applied successfully to determine a nucleation and subsequent bulk layer formation in the a-Si:H deposition.[10,11] In addition, based on the change in the dielectric function at the interface, the characterization of p/i interfaces has also been made using SE.[12–13] The combination of real time SE with IR spectroscopy, therefore, gives us a new capability to determine the correlation of the microscopic structural evolution with the SiH$_n$ ($n=1\sim3$) local bonding states during the interface formation. Recently, this combination was adopted in the real-time studies of a-Si:H growth by reactive magnetron sputtering[7] and inductively coupled plasmas.[14]

For the structural characterization of the thin-interface layer, monolayer sensitivity is required in these real time monitoring techniques. In general, the real time application of IR spectroscopy is more difficult than that of SE in the UV/visible region. This originates from the fact that the extinction coefficient of a-Si:H films in the IR region ($k<0.1$ at 2000 cm^{-1}) is significantly smaller than that in the UV/visible region ($k<3$). Various approaches that have been used to increase the IR absorption signal include the application of a metal[4,5] or optical cavity substrate,[7] high-intensity IR sources,[9] and attenuated total reflection (ATR).[8,15] For the purpose of the a-Si:H interface layer study, IR spectroscopy performed by ATR is most promising owing to the very high sensitivity realized by the internal multiple reflection inside an ATR prism and a linear behavior of the IR absorbance over the film thickness.[8] So far, in the ATR measurement, monolayer sensitivity for the SiH$_n$ ($n=1\sim3$) surface mode on the H-terminated c-Si surface has been achieved.[15]

In this study, we have performed real time SE and ATR simultaneously during the a-Si:H deposition on the substrate, in an attempt to determine the interface layer forma-

tion mechanism. The microscopic structural evolution determined from SE showed an excellent correlation with the SiH$_n$ local bonding states observed in the ATR measurement. The combination of these real-time monitoring techniques provide an even greater ability to determine a depth-profile of the hydrogen content for the different SiH$_n$ ($n=1\sim2$) bulk bonding modes. As a result, we confirmed that the formation of a-Si:H islands consisting of SiH$_2$ bonds is responsible for the H-rich interface layer formation.

II. EXPERIMENT

We deposited an a-Si:H film by conventional parallel plate rf plasma-enhanced chemical vapor deposition (PECVD) using SiH$_4$ source gas at a near-surface substrate temperature of 240 °C. We determined this temperature by SE using the reported temperature response of the c-Si dielectric function.[16,17] In this PECVD system, the electrode spacing is 40 mm, and the diameter of each electrode is 10 cm. The rf power and pressure during the a-Si:H deposition are 1 W and 50 mTorr, respectively. This deposition condition yields the relatively slow a-Si:H deposition rate of 0.35 Å/s. In order to confirm the existence of the interface layer after the deposition of the 130 Å thick a-Si:H film, we performed a D_2 plasma treatment using rf power of 1 W, pressure of 50 mTorr, D_2 flow rate of 100 sccm, and substrate temperature of 200 °C. The a-Si:H film was deposited on a c-Si (100) substrate covered with a 30 Å-thick native oxide. We left this native oxide untreated to simulate the interface layer formation of an a-Si:H layer on oxide materials.

During the deposition of the a-Si:H film on the substrate, the real-time SE and ATR spectra were measured simultaneously. The SE was performed using a rotating-compensator instrument (J. A. Woollam, M-2000) that enables the measurement of ellipsometry parameters in the full range ($\Delta=0\sim360°$, $\psi=0\sim90°$). The measured photon energy in the SE spectra consists a total of 225 data points ranging from 1.7 to 5.0 eV. For real-time SE, we used a data acquisition time (t_a) of 1 s, and the spectra were measured continuously with a data repetition time (t_r) of 3 s. This measurement condition yields standard deviations of 0.05 (Δ) and 0.02 (ψ) at 3.0 eV. In a simplified one layer model (ambient/film/substrate), these standard deviations correspond to a thickness sensitivity of $\sim$0.1 Å. For the D_2 plasma treatment experiment, we used the longer t_a and t_r of 5 and 10 s, respectively. The analysis of the SE data acquired during the a-Si:H deposition was performed after the deposition using a two-layer model for the film consisting of [ambient/(surface roughness layer)/(bulk layer)/substrate].[10,11] The dielectric function of the surface roughness layer was modeled as a 50/50 vol.% mixture of the bulk layer material and voids, applying the Bruggeman effective medium approximation. The overall analysis procedure is made selfconsistently under the assumption that the dielectric function of the depositing film does not change within the analyzing film thickness. This analysis allows us to obtain a time evolution of the surface roughness layer thickness (d_s), bulk layer thickness (d_b), and the dielectric function of the film.

The real-time ATR spectra were measured by employing a Fourier-transform infrared instrument (Nicolet, Magna 560). The IR light is irradiated into the ATR prism through KRS-5 windows mounted on the deposition chamber at the incident angle of 45°, and detected by a Hg$_x$Cd$_{1-x}$Te detector. We measured the real time ATR spectra using p-polarized light, because an interference effect caused by the ambient/a-Si:H/c-Si multilayer structure can be eliminated in this configuration. In order to maximize the sensitivity of the ATR measurement, we used the relatively large c-Si ATR prism (80 mm×20 mm×1 mm). The total number of reflection on the effective surface area of 60×20 mm^2 in this ATR prism is 30. The measurement of the ATR spectra was performed using a spectra resolution of 8 cm^{-1} in the wavenumber range from 1500 to 4000 cm^{-1}. In our case, the lowest measurable range in the ATR spectra is limited by the onset of the strong absorption of the c-Si ATR prism. The real time ATR measurement during the a-Si:H deposition was performed with a t_a of 6 and a t_r of 7 s, respectively. This ATR measurement condition leads to a thickness resolution of $\sim$3 Å in the a-Si:H deposition at 0.35 Å/s. During the D_2 plasma treatment, these values are increased to 14.7 (t_a) and 15 s (t_r), respectively. The data analysis procedure in the real time ATR spectra includes a deconvolution analysis of the ATR absorbance spectra for the different SiH$_n$ ($n=1-2$) bonding states, and a conversion of each absorbance peak to the total hydrogen density (in units of cm^{-2}). From the slope of the total hydrogen density over the film thickness obtained from the SE analysis, we determined the depth profile of the hydrogen content for each SiH and SiH$_2$ bulk mode in the a-Si:H bulk layer. In this calculation, we used the atomic number density of 5.0×10^{22} cm^{-3} and the reported oscillator strength of 2.2×10^{20} and 9.0×10^{19} cm^{-2} for the SiH$_2$ bulk mode at 2100 cm^{-1} and the SiH bulk mode at 2000 cm^{-1}, respectively.[18] In this ATR data analysis, however, the thickness nonuniformity is expected to induce the error, since the thickness determined by SE is measured at the center position on the substrate, while the whole effective surface area on the substrate is detected in the ATR measurement. From the obtained thickness non-uniformity of a thick a-Si:H film ($\sim$3000 Å), we estimated this error to be $\sim$7%. The detail of the overall ATR data analysis procedure will be reported in a future paper. In order to confirm the validity of the ATR data analysis, we also measured the *ex situ* IR transmission spectra at room temperature and analyzed the data using the identical procedure reported previously.[18,19]

III. RESULTS AND DISCUSSION

A. Initial growth process of a-Si:H

Figure 1 shows the real-time ATR spectra measured during the first 4 min after initiating the a-Si:H deposition. In this figure, the absorbance of the real-time ATR spectra was obtained using the same IR transmission spectrum measured just before the a-Si:H deposition. This reference spectrum includes the feature of SiH$_4$ source gas absorption in the range form 2070 to 2300 cm^{-1} and most of the SiH$_4$ absorption can be removed from the ATR spectra by simply using this reference spectrum. Nevertheless, a small sharp spike with the absorbance of $\sim$0.001 at 2187 cm^{-1} can be seen in
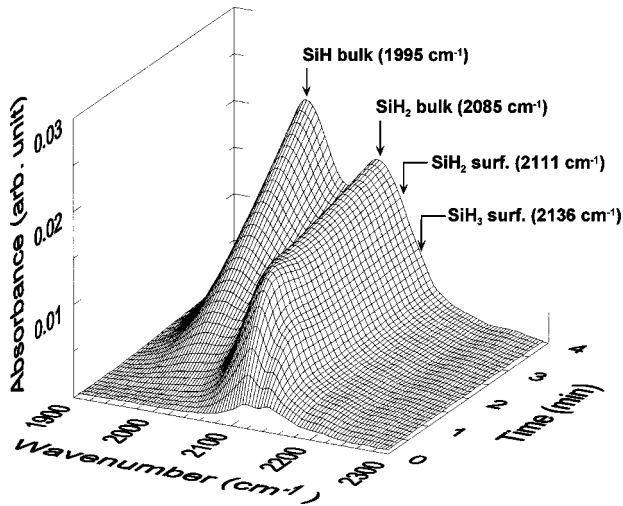
FIG. 1. Real-time ATR spectra measured during the first 4 min after initiating a-Si:H deposition.

the real-time ATR spectra due to the change in the partial pressure of SiH$_4$ by the plasma ignition. In the real-time ATR spectra shown in Fig. 1, we removed this feature consisting of three data points by a linear interpolation, for the purpose of the deconvolution analysis.

In the real-time ATR spectra measured before 0.5 min, two peaks at 2136 and 2111 cm^{-1} with the full width at half maximum (FWHM) of $\sim$27 cm^{-1} can be seen. Based on the studies of the H-terminated c-Si surface,[15] we assigned these two peaks to the SiH$_3$ and SiH$_2$ surface modes, respectively. This observation indicates that the surface of the a-Si:H during the deposition is covered with the SiH$_2$ and SiH$_3$ species at the deposition temperature of 240 °C. This result is consistent with our previous studies using IRRAS.[4,5] As the growth of the a-Si:H proceeds, the peak absorbance of the SiH$_2$ bulk mode at 2085 cm^{-1} rapidly increases up to $\sim$1 min, followed by a gradual increase observed after 1 min. The absorbance peak of the SiH bulk model at 1995 cm^{-1} also appeared at this time and increases almost linearly over the a-Si:H deposition time.

Figure 2 shows the real time ATR spectra corresponding
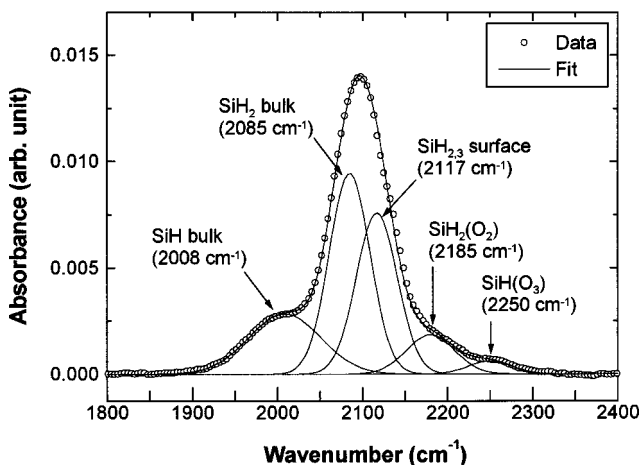
FIG. 2. Real-time ATR spectrum measured at 1.2 min after initiating a-Si:H deposition (open circle). The solid lines show the absorbance calculated by five Gaussian functions.

to 1.2 min in Fig. 1. At this deposition time, the SE analysis shows d_s and d_b of 16 and 12 Å, respectively. Here, we analyzed all the ATR spectra assuming five Gaussian functions as shown in Fig. 2. For the analysis of the SiH$_2$ and SiH$_3$ surface modes, we used a single Gaussian peak with a fixed peak position at 2117 cm^{-1} and FWHM of 57 cm^{-1} because of the large correlation of the SiH$_2$ surface mode at 2111 cm^{-1} with the SiH$_2$ bulk mode at 2085 cm^{-1}. In contrast, for the fitting of the SiH and SiH$_2$ bulk modes, we varied the peak positions and FWHM's as free parameters. The analysis for the two bulk modes show that the FWHM's are almost independent of the a-Si:H film thickness. In the initial stage of the a-Si:H deposition, however, we observed the clear peak shift for the SiH bulk mode from 2015 to 1995 cm^{-1}, while the SiH$_2$ bulk mode shows no such peak shift. This result will be discussed later in detail. In the deconvolution analysis of the ATR spectra, we also included two peaks at 2185 and 2250, which have been assigned to the SiH$_2$(O$_2$) and SiH(O$_3$).[20,21] The peak shift of these modes toward higher wave numbers, compared with the SiH(Si$_3$) and SiH$_2$(Si$_2$), has been explained by the induction effect; namely, the force constants of the IR atomic vibration increase by the bonding of the SiH to more electronegative atoms.[21] As shown in Fig. 2, the total sum of the five Gaussian peaks provides a good fitting to the measured real time spectra, supporting the validity of the deconvolution analysis.

Figure 3 shows the time evolution of the a-Si:H growth obtained from the analysis of SE (a) and ATR (b). In the early stage of the a-Si:H deposition ($t < 0.7$ min), the SE results show the rapid increase in d_s to $\sim$20 Å without the bulk layer formation ($d_b \sim 0$ Å). This result is consistent with the three-dimensional island growth of a-Si:H on c-Si native oxide substrate, and such a-Si:H island formation on various substrates has been supported by the results obtained from scanning tunneling microscopy,[22] atomic force microscopy,[23] and SE measurements.[11] At the deposition time of 0.7 min, the substrate surface is completely covered by a-Si:H islands, and the formation of the a-Si:H bulk layer occurs at the average growth rate of 0.35 Å/s. During the coalescence of a-Si:H islands, a clear surface smoothening of the a-Si:H layer due to the surface diffusion of the precursors can be seen. Similar behavior has already been observed in an SE study of a-Si:H deposition, and it has been reported that the surface smoothening enhancement leads to better electrical properties in the resulting a-Si:H films.[11]

Figure 3(b) shows the time evolution of the integrated absorbance obtained from the deconvolution analysis of the real-time ATR spectra. For the time evolution of the integrated absorbance of the SiH$_{2,3}$ surface modes, we found an excellent agreement with the variation in the surface roughness shown in Fig. 3(a). This result indicates that the absorbance intensity of the surface mode is proportional to the effective surface area or, in other words, that the a-Si:H surface is covered uniformly with these species. It should be mentioned that the results shown in Figs. 3(a) and 3(b) were obtained in completely separate measurements, and the common value in these measurements is only the deposition time. The surface smoothening observed by SE and ATR during the coalescence, therefore, strongly supports the exis-
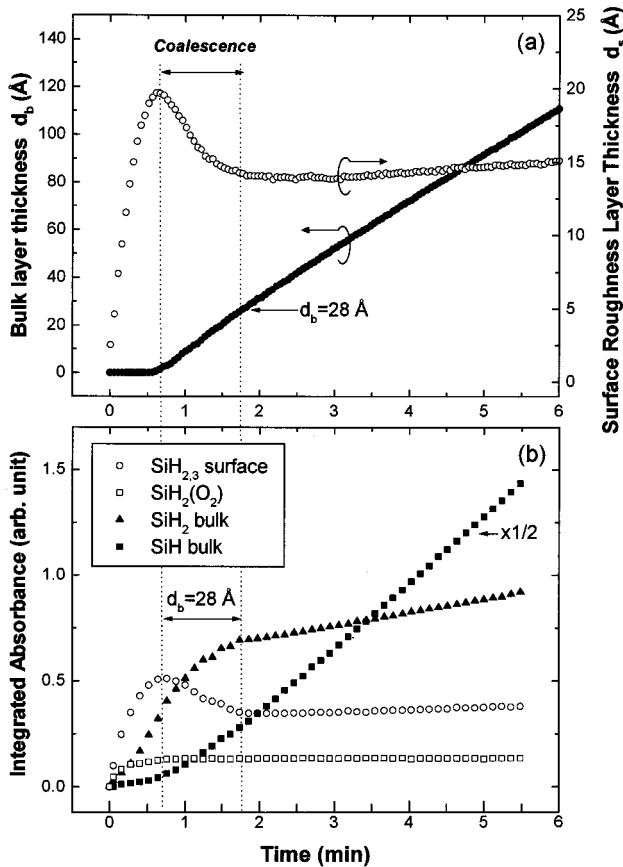
FIG. 3. Time evolution of the bulk layer thickness (d_b) and surface roughness layer thickness (d_s) determined by the SE analysis (a), and the integrated absorbance for the SiH$_n$ ($n=1\sim3$) bonds determined by the ATR analysis (b) during *a*-Si:H deposition on SiO$_2$/c-Si substrate. In (b), the integrated absorbance for the SiH bulk mode (solid square) is scaled down by half for clarity.

FIG. 4. Hydrogen content of the *a*-Si:H layer for the SiH and SiH$_2$ bulk modes (a), and the SiH peak position in the real time ATR spectra (b), plotted as a function of film mass thickness (d_f). The thickness d_f is calculated by $d_b+0.5d_s$ using the data shown in Fig. 3(a). In (b), the inset shows the SiH peak position plotted as a function of the total hydrogen content of the depositing *a*-Si:H layer.

tence of the surface diffusion process that enables the selective adsorption of the precursors at valleys where the sticking probability is higher than other parts. For the time evolution of the SiH$_2$(O$_2$), we found a clear saturation when the native oxide is covered with *a*-Si:H islands at 0.7 min. The result for the SiH(O$_3$) showed a similar trend as the SiH$_2$(O$_2$) but with smaller intensities. These results suggest that the SiH$_2$(O$_2$) and SiH(O$_3$) are formed by the hydrogenation of the native oxide surface and remain at the interface.

As evidenced in Fig. 3(b), in the island formation regime ($t<0.7$ min), the integrated absorbance of the SiH$_2$ bulk mode is dominant, while that of the SiH bulk mode is almost negligible. This result shows that *a*-Si:H islands on the substrate consists mainly of SiH$_2$ bonds. In the following coalescence regime ($0.7<t<1.8$ min), in contrast, the absorbance of the SiH bulk mode gradually increases, while the incorporation of SiH$_2$ bonds decreases. After the end of coalescence at 1.8 min ($d_b=28$ Å), the *a*-Si:H growth reaches the steady-state and the integrated absorbance for each bulk mode increases almost linearly. From the results mentioned above, it is evident that a ~30 Å-thick interface layer having a large amount of SiH$_2$ bonds is formed on the substrate in the early deposition process.

Figure 4 shows the hydrogen content of the *a*-Si:H bulk layer (a) and the SiH peak position (b) plotted as a function of the film mass thickness (d_f). Here, d_f is defined as the total volume of the *a*-Si:H film and is calculated from $d_b+0.5d_s$ using the data shown in Fig. 3(a). As mentioned earlier, the hydrogen content for each SiH and SiH$_2$ bulk mode is determined from the slope of the total hydrogen density over d_f. In this analysis, we obtained the slope at each point by performing a first-order regression analysis using five data points. From the number of the data points used in the regression analysis, we estimated the depth resolution in this analysis to be ~10 Å. As shown in Fig. 4(a), the hydrogen content from the SiH$_2$ shows a rapid increase with a negligible amount of the SiH during the *a*-Si:H island formation ($d_f<10$ Å). During the coalescence process ($10<d_f<35$ Å), the hydrogen content from the SiH$_2$ decreases gradually, while the SiH hydrogen content increases. When the substrate is completely covered with *a*-Si:H islands ($d_f=10$ Å), we obtained the maximum total hydrogen content of 37 at. %. This maximum value is, however, depth-resolution limited and increases further to 50 at. % upon performing the first-order regression analysis using two data points (depth resolution is ~3 Å). By taking the average, we determined the hydrogen content of the interface layer ($d_f=35$ Å or $d_b=28$ Å) to be 17 at. %. In the steady-state

a-Si:H deposition ($d_f > 35$ Å), the SiH$_2$ hydrogen content is only 1 at. % with the SiH hydrogen content of 9 at. %. The average hydrogen contents in the 3000 Å thick a-Si:H film measured by the *ex situ* transmission measurement are 10 and 1 at. % for the SiH and SiH$_2$ bulk modes, respectively, and agrees well with the ATR results.

The above results show that the interface layer formation is primarily caused by the deposition of porous a-Si:H islands in which SiH$_2$ bonds are dominant. Furthermore, it is evident that a rapid a-Si:H network formation occurs during the coalescence of a-Si:H islands. As shown in Fig. 3(a), this process is accompanied by the surface smoothening of the a-Si:H layer. This evidence is consistent with our idea that the surface diffusion of the precursors on the a-Si:H surface promotes a dense a-Si:H network formation.[24]

As confirmed from Fig. 4(b), the SiH peak position shifts to lower wave numbers with increasing d_f and reaches $\sim$1995 cm^{-1} after the end of the coalescence process ($d_f = 35$ Å). It should be mentioned that the *ex situ* IR transmission spectrum shows peak positions at 2000 and 2090 cm^{-1} for the SiH and SiH$_2$ bulk modes, respectively. The peak shift of $\sim$5 cm^{-1} observed in each bulk mode at room temperature is, therefore, due to the temperature effect and agreed well with the calculated peak shift of $\sim$7 cm^{-1} using the reported temperature coefficient of 0.035 cm^{-1}/K.[25] The peak shift of the SiH bulk mode shows a good correlation with the rapid decrease in the total hydrogen content. In addition, we found an almost linear dependence of the SiH peak position on the total hydrogen content as shown in the inset of Fig. 4(b). A similar dependence of the SiH peak position on the hydrogen content of the a-Si:H film was also reported previously.[26] The above results are quite indicative that the observed large peak shift of $\sim$20 cm^{-1} for the SiH bulk mode is induced by a rapid change in the local a-Si:H network structure surrounding the SiH bonds. Theoretically, the shift in the SiH peak position has been explained by the depolarization of the electric field in solid a-Si:H,[27] and is given by

$$\omega_{\text{Si-H}} = \omega_0 - \frac{e^{*2}}{2mR^3\omega_0}\frac{\varepsilon-1}{2\varepsilon+1}, \tag{1}$$

where e^*, m, R, and ε are the dynamical charge of the dipole, the reduced mass equivalent to hydrogen, the spherical cavity radius, and the dielectric constant, respectively. In this model, the peak position of the SiH stretching mode calculated by the valence force field model ($\omega_0 = 2100$ cm^{-1}) shifts to a lower wave number due to the depolarization effect of the vibrating dipole in the solid. Assuming $e^* = 0.4e$, $\varepsilon = 12$, and $R = 1.17$ Å, this model was used successfully to explain the peak position of the SiH stretching mode at $\sim$2000 cm^{-1}.

According to this model, the shift of the SiH peak toward the higher wave number can be explained by the decrease in the dielectric constant. Nevertheless, this assumption is not proper in our case, because we have to assume the unrealistic ε of 4 to account for the observed peak shift of 20 cm^{-1}. In the H-rich a-Si:H layer, the R value is also expected to change, since the optical cavity for the depolarization field becomes larger in a porous film structure. As shown in Eq.

(1), R has a strong influence on the peak shift and the R variation by $\sim$0.1 Å is sufficient to induce a peak shift of 20 cm^{-1}. The other possible explanation is the peak shift by the dynamical charge variation. As discussed previously,[18] the dynamical charge is comprised by the dynamic term and the static term, which are attributed to the atomic vibration and electronegatively, respectively. Although the systematic study of each charge contributions has not been made, it is expected that the static charge may change in the H-rich Si network owing to the higher electronegativity of H than Si (1.8 for Si, 2.1 for H). As discussed above, it is difficult to predict the possible peak position from Eq. (1) since the formation of the H-rich Si network is considered to vary e^*, R, and ε simultaneously. On the contrary, we can use the SiH peak position itself as a good indicator to express the local environment of the SiH bonds, provided that the SiH peak position always shifts to a higher wavenumber as the a-Si:H network becomes more porous and H-rich.

B. D_2 plasma treatment of a-Si:H layer

From the SE and ATR results shown above, the H-rich layer formation is evident during the initial nucleation of a-Si:H islands on the substrate. Nevertheless, there is a possibility that the 35 Å-thick SiH$_2$ layer on the substrate was divided into interface and surface layers in the a-Si:H deposition process that occurred after the interface formation. In order to verify the contribution of the SiH$_2$ layer at the near-surface, we performed a D_2 plasma treatment of the deposited 130 Å-thick a-Si:H layer. This experiment is based on the idea that, if most of the H-rich interface layer locates near the surface, the integrated absorbance of the SiH$_2$ bulk mode should disappear more rapidly than that of the SiH bulk mode having the uniform hydrogen content, since the H-D exchange reaction takes place from the surface.

Figure 5 shows the analysis results obtained from SE (a) and ATR (b) during D_2 plasma treatment. In this SE analysis, the dielectric function of the a-Si:H extracted during the a-Si:H deposition is used. The SE result shown in Fig. 5(a) reveals a strong etching behavior of the a-Si:H layer by the D_2 plasma even at the relatively low rf power of 1 W. We found that this etching process is accompanied by surface roughening from an initial value of 15 Å to a maximum of 30 Å. Figure 5(b) shows the variation in the integrated absorbance for the SiH$_2$ and SiH bulk modes determined from the deconvolution analysis. As shown in Fig. 5(b), the SiH integrated absorbance shows a rapid decay after initiating the D_2 plasma treatment and reaches almost to zero at 10 min ($d_b = 75$ Å). This result indicates that the diffusion of deuterium is much faster than the observed etching process. In contrast, the integrated absorbance of the SiH$_2$ bulk mode showed a much slower decay compared with the SiH case. Since the SiH$_2$ hydrogen content in the a-Si:H bulk layer ($\sim$1 at. %) is significantly lower than that of the interface layer ($\sim$17 at. %), it is obvious from above results that most of the H-rich layer remains at the interface region.

From the data shown in Fig. 5(b), we further carried out a quantitative analysis, assuming that a diffusion profile of deuterium can be calculated by the standard error-function-complement (erfc) form. In this calculation, the native oxide
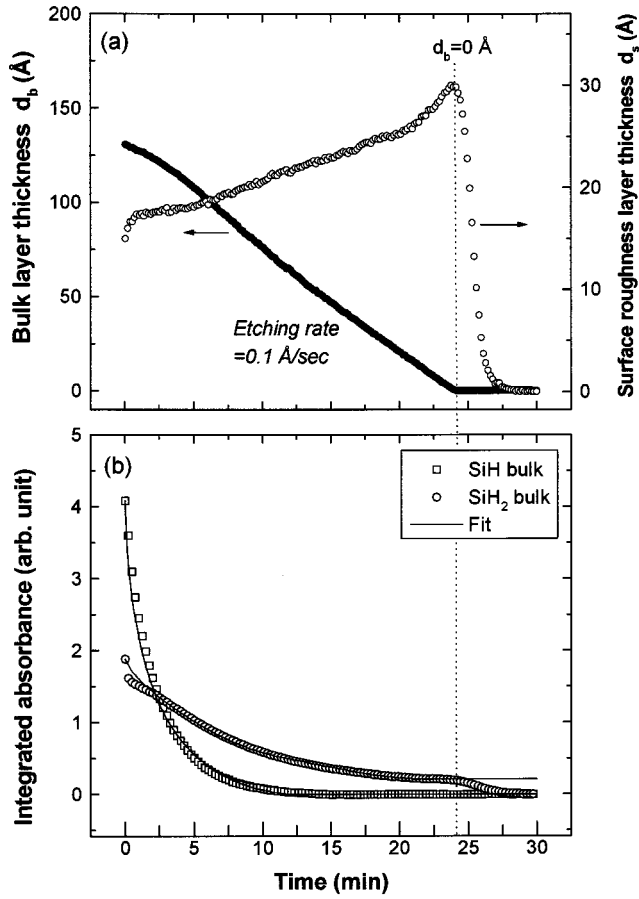
FIG. 5. Time evolution of the bulk layer thickness (d_b) and surface roughness layer thickness (d_s) determined by the SE analysis (a), and the integrated absorbance for the SiH and SiH$_2$ bulk modes determined by the ATR analysis (b) during D_2 plasma treatment of the 130 Å-thick a-Si:H film. In (b), the solid lines show the variations calculated by the deuterium diffusion profile assuming a error-function complement.

of c-Si is treated as a diffusion barrier, and we include the etching effect of the a-Si:H layer. Under these assumptions, the integrated absorbance at time t is expressed by

$$I(t) = I_{tot} - \left[\int I_0 \, \text{erfc}\left(\frac{z}{2\sqrt{Dt}}\right) dz + I_0 r t \right], \qquad (2)$$

where I_{tot}, I_0, and r are total integrated absorbance, integrated absorbance for unit thickness, and etching rate, respectively. We fit the data for the SiH by Eq. (2) using a single-diffusion constant D as a free parameter. From the fitting, we obtained $D = 1.6 \times 10^{-15}$ cm^2/s, and this calculation result is shown as a solid line in Fig. 5(b). The obtained diffusion constant falls within the reported values ranging from 10^{-14} to 10^{-16} cm^2/s at this substrate temperature.[28]

For the fitting of the SiH$_2$ bulk mode, we modified Eq. (2) slightly owing to the inhomogeneous SiH$_2$ distribution for the thickness z. In this calculation, we used a multilayer model consisting of a 35 Å-thick interface layer and a 95 Å-thick a-Si:H bulk layer that have different I_0. The loss of the integrated absorbance by the H-D exchange reaction was determined by obtaining the area where $I_0(z)$ overlaps with

the profile calculated by the erfc function. By setting $D = 1.3 \times 10^{-16}$ cm^2/s, we obtained a good fitting for the variation of the SiH$_2$ mode as shown in Fig. 5(b). The obtained D for the SiH$_2$ mode is one order of magnitude slower than the one for the SiH, and it is rather strange to set the different diffusion constant for each bonding state. In the c-Si surface studies, however, a slower H-D exchange rate for the surface SiH$_2$ bonds than the surface SiH bonds was reported.[29] This effect has been attributed to the smaller cross section of the SiH$_2$ for the exchange reaction,[29,30] and a similar effect may account for the slower diffusion coefficient of the SiH$_2$ bulk bonds in our study.

It should be emphasized that we could not obtain a reasonable fitting with a model that the H-rich layer exists at the near-surface even when a slower diffusion constant was used. These results strongly support the H-rich interface layer formation on the substrate. Nevertheless, a rapid delay of the integrated absorbance for the SiH$_2$ mode observed at $t < 2.5$ min cannot be explained by the uniform distribution of SiH$_2$ bonds at the near-surface, and suggests the existence of a surface SiH$_2$ layer in a much thinner thickness than the interface layer. In addition, when the a-Si:H bulk layer is almost etched at 24 min, there is a small decay in the interface region. This behavior indicates that the etching of SiH$_2$ bonds, rather than the deuterium exchange reaction, causes this change. The generation of the isolated SiH$_2$ bonds at the interface may be responsible for the observed variation.

IV. CONCLUSION

We have applied the real time spectroscopic ellipsometry (SE) and infrared attenuated total reflection spectroscopy (ATR) to observe the interface layer formation of an a-Si:H film on a c-Si substrate covered with native oxide in a conventional rf plasma-enhanced chemical vapor deposition. From these real time monitoring techniques, we confirmed that the 35 Å-thick SiH$_2$ layer having the average hydrogen content of $\sim$17 at % is formed on the substrate. We also found the surface SiH$_2$ layer but with lesser hydrogen content and thickness compared with the interface layer. The interface layer formation is primarily caused by the formation of the H-rich a-Si:H islands deposited on the c-Si native oxide substrate. During the coalescence of three-dimensional islands, a significant a-Si:H network formation, accompanied by the surface smoothening, was found. This fact supports our idea that the surface diffusion of precursors promotes a dense a-Si:H network formation. In this study, a capability to determine the depth-profile of hydrogen content for the SiH and SiH$_2$ bulk bonds was presented by combining real time SE and ATR and this capability is promising for obtaining a good correlation of a-Si:H structural evolution with the SiH$_n$ local bonding states.

[1] K. S. Lim, M. Konagai, and K. Takahashi, J. Appl. Phys. **56**, 538 (1984).

[2] R. R. Ayra, A. Catalano, and R. S. Oswald, Appl. Phys. Lett. **49**, 1089 (1986).

[3] H. Ihara and H. Nozaki, Jpn. J. Appl. Phys., Part 2 **29**, L2159 (1990).

[4] Y. Toyoshima, K. Arai, A. Matsuda, and K. Tanaka, Appl. Phys. Lett. **56**, 1540 (1990).

[5] Y. Toyoshima, K. Arai, A. Matsuda, and K. Tanaka, J. Non-Cryst. Solids **137&138**, 765 (1991).

[6] R. Ossikovski and B. Drevillon, Phys. Rev. B **54**, 10 530 (1996).

[7] M. Katiyar, Y. H. Yang, and J. R. Abelson, J. Appl. Phys. **77**, 6247 (1995).

[8] S. Miyazaki, Y. Yoshida, Y. Miyoshi, and M. Hirose, Sol. Energy Mater. Sol. Cells **49**, 45 (1997).

[9] R. Ossikovski, H. Shirai, and B. Drevillon, Thin Solid Films **234**, 363 (1993).

[10] I. An, Y. M. Li, C. R. Wronski, H. V. Nguyen, and R. W. Collins, Appl. Phys. Lett. **59**, 2543 (1991).

[11] J. Koh, Y. Lee, H. Fujiwara, C. R. Wronski, and R. W. Collins, Appl. Phys. Lett. **73**, 1526 (1998).

[12] H. Fujiwara, J. Koh, C. R. Wronski, and R. W. Collins, Appl. Phys. Lett. **72**, 2993 (1998).

[13] H. Fujiwara, J. Koh, C. R. Wronski, and R. W. Collins, Appl. Phys. Lett. **74**, 3687 (1999).

[14] D. C. Marra, E. A. Edelberg, R. L. Naone, and E. S. Aydil, J. Vac. Sci. Technol. A **16**, 3199 (1998).

[15] Y. J. Chabal, G. S. Higashi, K. Raghavachari, and V. A. Burrows, J. Vac. Sci. Technol. A **7**, 2104 (1989).

[16] P. Lautenschlager, M. Garriga, L. Vina, and M. Cardona, Phys. Rev. B **36**, 4821 (1987).

[17] G. E. Jellison, Jr. and F. A. Modine, J. Appl. Phys. **76**, 3758 (1994).

[18] A. A. Langford, M. L. Fleet, B. P. Nelson, W. A. Lanford, and N. Maley, Phys. Rev. B **45**, 13 367 (1992).

[19] N. Maley, Phys. Rev. B **46**, 2078 (1992).

[20] M. Niwano, J. Kageyama, K. Kurita, K. Kinashi, I. Takahashi, and N. Miyamoto, J. Appl. Phys. **76**, 2157 (1994).

[21] G. Lucovsky, Solid State Commun. **29**, 571 (1979).

[22] K. Ikuta, K. Tanaka, S. Yamasaki, K. Miki, and A. Matsuda, Appl. Phys. Lett. **65**, 1760 (1994).

[23] H. N. Wanka, A. Hierzenberger, and M. B. Schubert, *Amorphous Silicon Technology*, edited by M. Hack, E. A. Schiff, N. Powell, A. Matsuda, and A. Madan, MRS Symposia Proceedings No. 377 (Materials Research Society, Pittsburgh, 1995), p. 263.

[24] A. Matsuda, K. Nomoto, Y. Takeuchi, A. Suzuki, A. Yuuki, and J. Perrin, Surf. Sci. **227**, 50 (1990).

[25] O. Grimal, D. P. Masson, L. Betrand, and A. Yelon, Phys. Rev. B **49**, 10 242 (1994).

[26] D. V. Tsu and G. Lucovsky, J. Non-Cryst. Solids **97&98**, 839 (1987).

[27] M. Cardona, Phys. Status Solidi B **118**, 463 (1983).

[28] W. B. Jackson and C. C. Tsai, Phys. Rev. B **45**, 6564 (1992).

[29] D. D. Koleske, S. M. Gates, and B. Jackson, J. Chem. Phys. **101**, 3301 (1994).

[30] E. Srinivasan, H. Yang, and G. N. Parsons, J. Chem. Phys. **105**, 5467 (1996).